Early time kinetics of systems with spatial symmetry breaking

Rachele Dominguez[*]

Department of Physics, Boston University, Boston, Massachusetts 02215, USA

Kipton Barros and W. Klein

Department of Physics and Center for Computational Science, Boston University, Boston, Massachusetts 02115, USA

In this paper we present a study of the early stages of unstable state evolution of systems with spatial symmetry changes. In contrast to the early time linear theory of unstable evolution described by Cahn, Hilliard, and Cook, we develop a generalized theory that predicts two distinct stages of the early evolution for symmetry-breaking phase transitions. In the first stage the dynamics is dominated by symmetry-preserving evolution. In the second stage, which shares some characteristics with the Cahn-Hilliard-Cook theory, noise-driven fluctuations break the symmetry of the initial phase on a time scale which is large compared to the first stage for systems with long interaction ranges. To test the theory we present the results of numerical simulations of the initial evolution of a long-range antiferromagnetic Ising model quenched into an unstable region. We investigate two types of symmetry-breaking transitions in this system: disorder-to-order and order-to-order transitions. For the order-to-order case, the Fourier modes evolve as a linear combination of exponentially growing or decaying terms with different time scales.

PACS number(s): 64.70.K−, 75.50.Ee, 64.60.De

I. INTRODUCTION

Many systems have effective long-range interactions and exhibit a variety of crystalline phases. Some examples are metals [1], block copolymers [2], and systems with modulated phases [3–5]. The kinetics of the transitions from a disordered spatially uniform state to a spatially periodic state (disorder to order) has been explored in several contexts (see, for example, Refs. [6–9]). Some aspects of the kinetics from one spatially periodic state to another (order to order) have also been investigated [10–12].

For systems with long-range interactions the phase ordering process is separated into an early time regime described by a linear theory, an intermediate regime where nonlinear effects first become important, and a late stage domain coarsening regime. Phase ordering, a process whereby a disordered state evolves into a state with macroscopic regions of like components, has been well studied for systems described by a Landau-Ginzburg free energy, such as the ferromagnetic Ising model [13]. If the coarse-grained order parameter is locally conserved, the phase ordering process is called spinodal decomposition. If it is not conserved, the process is called continuous ordering. The latter case is referred to as model A and the former is referred to as model B [14].

"Phase ordering" as used here is distinct from a disorder-to-order transition, which we take to mean a transition from a disordered to a spatially periodic state. A disorder-to-order transition breaks spatial symmetry; that is, the initial state has a spatial symmetry that is absent in the final state. In contrast, phase ordering for the ferromagnetic Ising model with a nonconserved order parameter has uniform spatial symmetry in both the initial and final phases. Thus, in this case phase ordering does not break spatial symmetry [15].

The early time linear regime of phase ordering was first studied by Cahn and Hilliard [16–18] and later by Cook [19]. This Cahn, Hilliard, and Cook (CHC) linear theory was originally developed to describe spinodal decomposition for systems such as binary alloys, where the order parameter is locally conserved. The CHC theory predicts exponential growth of certain Fourier modes immediately after a temperature quench into the unstable regime [16–19]. For systems with long-range interactions, this exponential growth lasts for a time proportional to the logarithm of the interaction range [20].

The CHC theory also describes continuous ordering for systems such as the ferromagnetic Ising model with a non-conserved order parameter. In this case the temperature is quenched to below the critical temperature at zero external field (a critical quench). However, if the external field is nonzero during the temperature quench (an off-critical quench), the CHC theory is not applicable. We will show that the CHC theory also fails to describe a wide class of transitions that break spatial symmetry.

In this paper we extend the CHC theory to describe transitions that break spatial symmetry and whose dynamics do not conserve the order parameter [21]. For these systems we find two distinct stages of the early time evolution in contrast to CHC. Stage one, which is absent in the CHC theory, is dominated by symmetry-preserving dynamics. The time scale for which this stage applies is independent of the interaction range. Stage two is analogous to the early time evolution described by CHC because the dynamical equations are characterized by exponential solutions, and the time scale for which stage two is valid is longer for longer interaction ranges. For disorder-to-order transitions certain Fourier modes grow exponentially. In contrast, for order-to-order transitions the Fourier modes evolve as a linear combination of exponentially growing or decaying terms with different time scales.
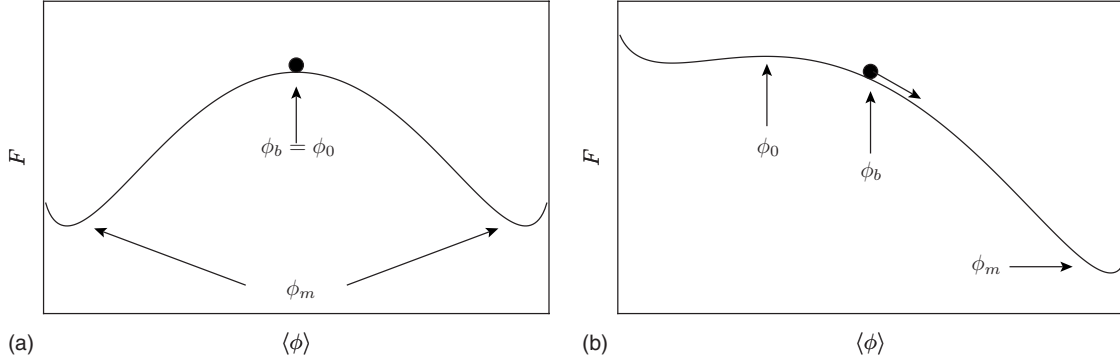
---
[*]erdomi@bu.edu

FIG. 1. A representation of the free-energy landscape for a ferromagnetic Ising model as a function of the average magnetization $\langle\phi\rangle$ for (a) a critical quench and (b) an off-critical quench for $h_f>0$. The dot represents the background configuration of the system immediately after the quench. For a critical quench the system is initially at an unstable stationary point of the free energy and the CHC theory governs its early evolution. For long-range systems the noise is effectively small, and the system fluctuates about the top of the hill for an extended time. Eventually, the system will be in one of the two global minima ϕ_m if the system size and temperature are finite. For an off-critical quench the background configuration sits to the right of the free-energy stationary point. The noiseless dynamics of Eq. (10) drives the system directly toward the stable minimum ϕ_m and away from the stationary point. Thus, in this case we do not expect stage two exponential growth at any time after the quench.

Our particular system of interest is the long-range antiferromagnetic Ising model. This system has spatial symmetry-breaking disorder-to-order and order-to-order transitions. We use Monte Carlo techniques to simulate the system and compare our results to our numerical solutions of a Langevin equation and to our analytical predictions.

The structure of this paper is as follows. Section II summarizes the theoretical background on unstable state evolution for models described by a Landau-Ginzburg free energy, focusing on the linear CHC theory. We extend this theory to include symmetry-breaking transitions in Sec. III. The role that symmetry breaking plays in the interplay between the two stages is discussed. The long-range antiferromagnetic Ising model and its phase diagram are introduced in Sec. IV. We develop the generalized theory for this model by using the Langevin equation based on a coarse-grained free energy as well as the Langevin equation describing Glauber dynamics. Our numerical and theoretical results are presented for the disorder-to-order case in Sec. V and for the order-to-order case in Sec. VI. Section VII summarizes and discusses our results.

II. REVIEW OF THE CHC THEORY FOR CONTINUOUS ORDERING

In this section we review the results of the CHC theory as they are applied to continuous ordering for which the order parameter is not conserved. We consider systems described by the Landau-Ginzburg free energy,

$$F[\hat{\phi}(x)] = \int dx\left\{\frac{R^2}{2}[\nabla\hat{\phi}(x)]^2 + \frac{\epsilon}{2}\hat{\phi}^2(x) + \frac{1}{4}\hat{\phi}^4(x) - h\hat{\phi}(x)\right\},$$

(1)

where $\epsilon=(T-T_c)/T_c$ is the reduced temperature, T_c is the critical temperature, h is the external field, and R is the interaction range. The evolution of these systems can be de-

scribed by a Langevin equation for the evolution of the order parameter $\hat{\phi}(x,t)$,

$$\frac{\partial\hat{\phi}(x,t)}{\partial t} = -M\left(\frac{\delta F[\hat{\phi}]}{\delta\hat{\phi}(x)}\right) + \sqrt{2MT}\,\eta(x,t),$$

(2)

where M is the mobility (which for the CHC theory is assumed to be a constant in space and time), $\eta(x,t)$ represents white Gaussian noise, and we have set $k_B=1$.

The CHC theory predicts the early stage evolution of the structure factor following a critical quench; that is, the temperatures before and after the quench satisfy $\epsilon_i>0$ and $\epsilon_f<0$, respectively, while the external field is held constant at zero. The result for the structure factor $S(k,t)=\langle\hat{\phi}(k,t)\hat{\phi}(-k,t)\rangle/V$ for early times is

$$S(k,t) = e^{2D_{\text{CHC}}(k)t}\left[S(k,t=0) + \frac{M}{\beta_f D_{\text{CHC}}(k)}\right] - \frac{M}{\beta_f D_{\text{CHC}}(k)},$$

(3)

where

$$D_{\text{CHC}}(k) = -M(R^2k^2 - |\epsilon_f|)$$

(4)

and $\beta_f=T_f^{-1}$. We see from Eq. (3) that the individual Fourier modes evolve independently of one another and that modes grow exponentially if $D_{\text{CHC}}(k)>0$.

Systems with $R\gg1$ are said to be near mean field and the limit $R\to\infty$ is the mean-field limit [22]. For $T_f<T_c$ simulations have shown that Eq. (3) is applicable for systems with $R\gg1$ for some initial time after the quench [23–26]. Binder [20] argued that the linear theory should break down when the fluctuations are large in comparison to the average order parameter. He predicted that the CHC theory breaks down at a time τ that scales as $\tau\sim\ln R$.

The result that the duration of applicability of the linear theory is longer for larger R is illuminated by a simple mechanical analogy (see Fig. 1). The CHC theory describes the evolution of certain fluctuations of the system about an un-

stable stationary point of the free energy. The system is analogous to a ball sitting at the top of a fairly flat hill subject to small random perturbations. These perturbations will eventually cause the ball to roll off the hill; the smaller the perturbations, the longer it takes for the ball to roll off. As R increases the noise effectively decreases and the system remains near the unstable point of the free energy longer. When the free energy can no longer be approximated quadratically, the CHC theory is no longer valid.

III. GENERALIZATION OF THE CHC THEORY

We consider a Langevin equation of the general form

$$\frac{\partial \phi(\mathbf{r},t)}{\partial t} = \Theta[\phi,\mathbf{r}] + \sqrt{B[\phi,\mathbf{r}]} R^{-d/2} \eta(\mathbf{r},t), \qquad (5)$$

where $\phi(\mathbf{r},t)$ is the order parameter with scaled coordinates ($\mathbf{r} \equiv \mathbf{x}/R$ and $\mathbf{q} \equiv \mathbf{k}R$) and the drift term $\Theta[\phi,\mathbf{r}]$ is nonlinear in $\phi(\mathbf{r},t)$. $B[\phi,\mathbf{r}]$ is a noise parameter to be determined by a fluctuation-dissipation theorem, and the noise satisfies

$$\langle \eta(\mathbf{r},t) \rangle = 0, \qquad (6)$$

$$\langle \eta(\mathbf{r},t) \eta(\mathbf{r}',t') \rangle = \delta(\mathbf{r} - \mathbf{r}') \delta(t - t'). \qquad (7)$$

Equation (5) is written in scaled coordinates so that the R dependence of the noise term is explicit.

The CHC theory utilizes an expansion about a uniform order-parameter background. This background configuration is time independent after a critical quench. More generally, we will expand about a background configuration $\phi_b(\mathbf{r},t)$ which is not necessarily uniform and may be time dependent after the quench.

At the time of the quench, the system is in a configuration consistent with the equilibrium state before the quench. We can write this state as $\phi(\mathbf{r},t=0) = \phi_b(\mathbf{r},t=0) + R^{-d/2} \psi(\mathbf{r},t=0)$. The background configuration $\phi_b(\mathbf{r},t=0)$ is a solution to the Euler-Lagrange equation for T_i and h_i, is independent of the noise, and may be nonuniform. The term $R^{-d/2} \psi(\mathbf{r},t=0)$ represents small fluctuations about the background due to the noise. In general, $\phi_b(\mathbf{r},t=0) \neq \phi_0(\mathbf{r})$; that is, the background configuration is not a stationary point of the free energy and may be time dependent after the quench. We are interested in how this background configuration and these fluctuations evolve with time after the quench, which is the time evolution of

$$\phi(\mathbf{r},t) = \phi_b(\mathbf{r},t) + R^{-d/2} \psi(\mathbf{r},t). \qquad (8)$$

If we expand Eq. (5) to first order in the small fluctuations, $R^{-d/2} \psi(\mathbf{r},t)$, about the background configuration $\phi_b(\mathbf{r},t)$, we obtain

$$\frac{\partial \phi_b(\mathbf{r},t)}{\partial t} + R^{-d/2} \frac{\partial \psi(\mathbf{r},t)}{\partial t}$$
$$= \Theta[\phi,\mathbf{r}]\big|_{\phi=\phi_b} + \int d\mathbf{r}' \left. \frac{\delta \Theta[\phi,\mathbf{r}]}{\delta \phi(\mathbf{r}',t)} \right|_{\phi=\phi_b} R^{-d/2} \psi(\mathbf{r}',t)$$
$$+ \sqrt{B[\phi,\mathbf{r}]}\big|_{\phi=\phi_b} R^{-d/2} \eta(\mathbf{r},t). \qquad (9)$$

It is natural to separate Eq. (9) terms of order R^0 from terms of order $R^{-d/2}$, giving the dynamical equations for the background and the fluctuations [27]. The equation for the evolution of the background configuration, which is zeroth order in $R^{-d/2}$, is

$$\frac{\partial \phi_b(\mathbf{r},t)}{\partial t} = \Theta[\phi]\big|_{\phi=\phi_b} \quad \text{(evolution of background)}. \qquad (10)$$

Equation (10) is noiseless and independent of R. In contrast, the equation for the evolution of the fluctuations is noise driven and is first order in $R^{-d/2}$,

$$\frac{\partial \psi(\mathbf{r},t)}{\partial t} = \int d\mathbf{r}' \left. \frac{\delta \Theta[\phi,\mathbf{r}]}{\delta \phi(\mathbf{r}',t)} \right|_{\phi=\phi_b} \psi(\mathbf{r}',t)$$
$$+ \sqrt{B[\phi]}\big|_{\phi=\phi_b} \eta(\mathbf{r},t) \quad \text{(evolution of fluctuations)}. \qquad (11)$$

The background configuration $\phi_b(\mathbf{r},t)$ and the fluctuations $\psi(\mathbf{r},t)$ evolve simultaneously; Eqs. (10) and (11) together describe the early time kinetics of unstable systems. Equation (11) differs from the CHC theory described in Sec. II because the coefficient of $\psi(\mathbf{r},t)$ on the right-hand side of Eq. (11) depends on $\phi_b(\mathbf{r},t)$, which evolves according to Eq. (10). Because of the explicit time dependence of $\phi_b(\mathbf{r},t)$, we do not expect to find exponential solutions as found in the CHC theory.

Equation (10) dominates the evolution of $\phi(\mathbf{r},t)$ until $|\Theta[\phi]|_{\phi=\phi_b}| \sim R^{-d/2}$ (we will discuss specific examples of this evolution in the following). We refer to the kinetics while the background configuration is evolving as *stage one*. If

$$|\Theta[\phi]|_{\phi=\phi_b}| \ll R^{-d/2}, \qquad (12)$$

we refer to the kinetics as *stage two*.

If $\Theta[\phi] \propto \delta F/\delta \phi$, then Eq. (5) becomes a dissipative Langevin equation. In the limit $R \to \infty$ the condition for stage two evolution [Eq. (12)] implies that $\delta F/\delta \phi \simeq 0$ or

$$\phi_b(\mathbf{r},t) = \phi_0(\mathbf{r}), \qquad (13)$$

where $\phi_0(\mathbf{r})$ is an unstable solution to the Euler-Lagrange equation for the final parameters T_f and h_f corresponding to the temperature and external field after the quench, respectively. In stage two the dynamics shares several features with the dynamics of CHC. Namely, the background configuration is nearly a stationary point of the free energy, and the linear evolution admits (nearly) exponential solutions, which are applicable for a time $\tau \sim \ln R$.

If $\phi_b(\mathbf{r},t=0) \neq \phi_0(\mathbf{r})$, then stage one kinetics begins immediately after the quench and either there is no stage two kinetics at any time after the quench or stage two kinetics follows stage one. If $\phi_b(\mathbf{r},t=0) = \phi_0(\mathbf{r})$, then stage one kinetics is absent and stage two kinetics begins immediately after the quench. Table I summarizes the various possibilities.

A critical quench in the ferromagnetic Ising model [see Table I and Fig. 1(a)] exhibits stage two but not stage one kinetics. In this case $T_i = \infty$, $h_i = 0$, $T_f < T_c$, $h_f = 0$, and $\phi_b(t=0) = \phi_0$.

TABLE I. Summary of early kinetics for various types of transitions for the long-range ferromagnetic Ising model and the long-range antiferromagnetic Ising model. In this table $\phi_b(t=0)$ is the background configuration just after the quench and ϕ_0 is the unstable solution to the Euler-Lagrange equation for T_f and h_i. These quenches are defined in text.

Case	Spatial symmetry breaking	Stage one	Stage two	Example
$\phi_b(t=0) \simeq \phi_0$	No	No	Yes	Critical quench for ferromagnet
	Yes	No	Yes	Critical quench for antiferromagnet
$\phi_b(t=0) \neq \phi_0$	No	Yes	No	Off-critical quench for ferromagnet
	Yes	Yes	Yes	Off-critical and external field quench for antiferromagnet

In contrast, an off-critical quench in the ferromagnetic Ising model [see Table I and Fig. 1(b)] is an example that exhibits stage one but not stage two kinetics. In the off-critical quench the initial conditions are the same as for the critical quench ($T_i = \infty$ and $h_i = 0$), but the system is quenched below T_c and $h_f \neq 0$. Because $h_f \neq 0$, the initial background configuration $\phi_b(t=0) = 0$ is not a solution to the Euler-Lagrange equation for the final parameters T_f and h_f. The background configuration evolves via Eq. (10) directly toward the stable minimum ϕ_m of the free-energy landscape and away from the unstable solution ϕ_0 [see Fig. 1(b)]. Hence, the system will never reach the unstable stationary point and there will be no stage two kinetics.

In contrast to the ferromagnetic Ising model [28], we find stage one followed by stage two kinetics in systems that break spatial symmetry. In this case the noiseless dynamics in stage one and the initial configuration conspire to drive the configuration toward the unstable solution of the Euler-Lagrange equation ϕ_0. In stage one both $\phi_b(r)$ and $\psi(r,t)$ evolve simultaneously until the system reaches the unstable solution ϕ_0 for T_f and h_f. Stage one kinetics is analogous to a ball rolling down a hill toward a saddle point (see Fig. 2). When the system reaches the stationary point, stage two begins. Stage two is analogous to the ball fluctuating about the top of the hill and ends when the ball finally rolls off the top of the hill toward a stable state.

Why does the ball in Fig. 2 not roll off the hill before it reaches the saddle point? Symmetry considerations provide the answer. For dissipative dynamics where $\Theta \propto -\delta F / \delta \phi$, the noiseless dynamics of Eq. (10) preserves certain spatial symmetries, depending on the form of the free energy. The dynamics of Eq. (10) evolves $\phi_b(r,t)$ to the lowest free energy within these symmetry constraints. This configuration is an unstable stationary point of the free energy. It is a local minimum with respect to the symmetry-constrained degrees of freedom but a local maximum with respect to the other symmetry-breaking degrees of freedom. Once at this saddle point, the nonlinear background dynamics of stage one terminates and stage two kinetics takes over. See also Ref. [29].

The spatial symmetries preserved by the noiseless dynamics of Eq. (10) are not preserved by the noise-driven dynamics of Eq. (11); that is, the noise causes random fluctuations which break the spatial symmetries of $\phi_b(r,t)$. Initially, these spatial symmetries are broken by $\psi(r,t=0)$, the fluctuations about the background at the time of the quench due to $\eta(r,t<0)$, the noise in the system before the quench. These

initial fluctuations, which are of order $R^{-d/2}$, begin to grow (or decay) immediately after the quench according to Eq. (11). However, during stage one the fluctuations $\psi(r,t)$ remain of order $R^{-d/2}$. The reason the ball in Fig. 2 does not roll off the hill is because the fluctuations which would drive the ball off the hill are small for sufficiently large R. The time it takes for the ball to roll down to the saddle point (the duration of stage one) is independent of R. In stage two kinetics, when the nonlinear dynamics of Eq. (10) has ceased, the symmetry-breaking fluctuations continue to grow for an extended period of time, eventually becoming of the order 1.

IV. LONG-RANGE ANTIFERROMAGNETIC ISING MODEL

A. Model and phase diagram

To investigate a system with spatial symmetry-breaking phase transitions, we simulate the long-range antiferromag-
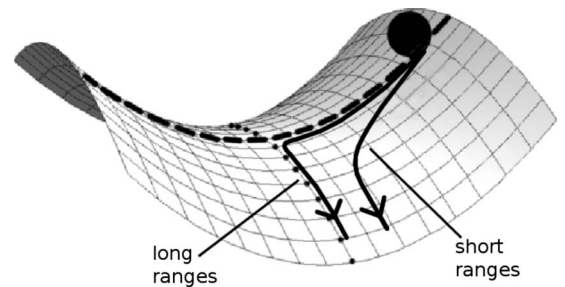

FIG. 2. A representation of the free-energy landscape for a system with spatial symmetry breaking. For systems with short-range interactions fluctuations cause the ball (representing the background configuration of the system) to roll off the hill, the ball does not approach the saddle point, and stage two behavior is not observed. In contrast, for systems with long-range interactions the evolution of fluctuations governed by Eq. (11) is suppressed by a factor of $R^{-d/2}$, and the noiseless dynamics of Eq. (10) dominates. Due to this noiseless symmetry-preserving dynamics the ball rolls down the hill toward the saddle point along the dashed line with little deviation due to the fluctuations. The dashed line represents all configurations with the same symmetry as the initial state. The directions perpendicular to the dashed line represent symmetry-breaking degrees of freedom. Once near the saddle point, the ball essentially stops rolling [condition (12) is satisfied] and stage two kinetics takes over as unstable fluctuations grow for a time of order $\tau \sim \ln R$. Eventually, after stage two, the ball will roll off the hill along the dotted line.
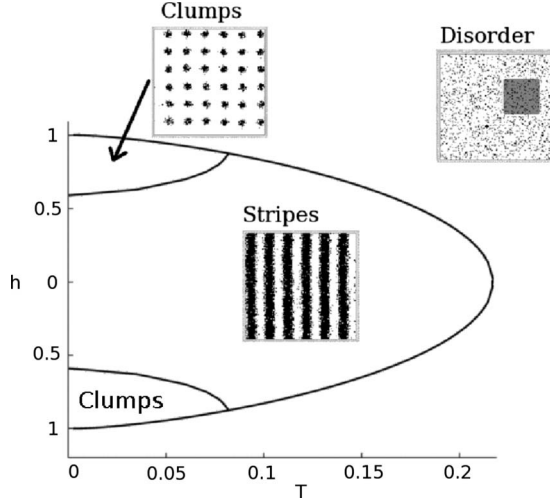
FIG. 3. Approximate phase diagram for the long-range antiferromagnetic Ising model with a square-shaped interaction. The system has two low-temperature ordered phases, the clump phase and the stripe phase, and a disordered phase. The darkened square in the snapshot of the disordered Ising model shows the interaction range for a spin at the center of the square.

netic Ising model using Glauber Monte Carlo dynamics [30]. Time is measured in units of Monte Carlo step (MCS) per spin. For N spins in a system, 1 MCS is equal to N spin-flip attempts. With this definition, it is natural to consider fractional Monte Carlo steps in which fewer than N spin flips have been attempted.

We study the two-dimensional long-range antiferromagnetic Ising model with a square-shaped interaction. For this interaction a spin at $\boldsymbol{x} = (x, y)$ interacts with a second spin at $\boldsymbol{x}' = (x', y')$ only if $|x - x'| \leq R$ and $|y - y'| \leq R$ (see Fig. 3).

There are two types of periodic low-temperature configurations, which we call the stripe phase and the clump phase, which are energetically favorable with respect to the disordered phase. The system can lower its overall interaction energy in the clump or stripe phases by grouping like spins together. Although a spin pays an energy cost due to its proximity to the other spins in its own clump or stripe, it avoids interacting with most of the spins in neighboring clumps or stripes. This system is related to a previously studied model of particles [31].

An approximate phase diagram is shown in Fig. 3. The pictures are snapshots of the configurations from our Monte Carlo simulations. From Fig. 3 we see that the disorder-to-clumps transition as well as the disorder-to-stripes transition is symmetry-breaking disorder-to-order transitions. In both cases the uniform spatial symmetry is lost. The two order-to-order transitions are also symmetry breaking. In the transition from stripes to clumps the continuous translational symmetry along the direction of the stripes is lost. In the clumps to stripes transition the 90° rotational symmetry is lost.

B. Dissipative Langevin dynamics

We now develop the equations for the relaxational Langevin dynamics as well as the background and fluctuation dynamics for a free energy which corresponds to the long-range antiferromagnetic Ising model. We begin with the coarse-grained free energy

$$F[\phi(\boldsymbol{r})] = R^d \left(-\frac{J}{2} \int d\boldsymbol{r}[(\Lambda * \phi)(\boldsymbol{r})]\phi(\boldsymbol{r}) \right.$$
$$\left. - \int d\boldsymbol{r}\{Ts[\phi(\boldsymbol{r})] + h\phi(\boldsymbol{r})\} \right), \qquad (14)$$

where $\phi(\boldsymbol{r}) = \frac{1}{(\Delta)^d}\Sigma_i S_i$ is the coarse-grained magnetization of the spins inside a box of length Δ in d dimensions centered at position $\boldsymbol{r}$. We use the notation $(\Lambda * \phi)(\boldsymbol{r}) \equiv \int d\boldsymbol{r}' \Lambda(\mathbf{r} - \boldsymbol{r}')\phi(\boldsymbol{r}')$ to denote a spatial convolution. $J = +1$ for the ferromagnet and $J = -1$ for the antiferromagnet. The entropy density $s[\phi(\boldsymbol{r})]$ due to the coarse-graining procedure is

$$s[\phi(\boldsymbol{r})] = 2 \ln 2 - \frac{1}{2}\{[1 + \phi(\boldsymbol{r})]\ln[1 + \phi(\boldsymbol{r})]$$
$$+ [1 - \phi(\boldsymbol{r})]\ln[1 - \phi(\boldsymbol{r})]\}. \qquad (15)$$

The scaling of the strength of the interaction is implicit in the interaction function $\Lambda(\boldsymbol{r})$ which we take to be a repulsive pairwise step potential of the form

$$\Lambda(x, y) = \begin{cases} 1/z & (-R \leq x, y \leq R) \\ 0 & \text{otherwise,} \end{cases} \qquad (16)$$

where z is the number of spins within the interaction region of a single spin and $z \sim (2R)^d$ for large R.

This form of the potential by Kac *et al.* [32] yields a Hamiltonian that is well defined in the mean-field limit; the energy per spin remains finite as $R \rightarrow \infty$ because $\int d\boldsymbol{r}\Lambda(\boldsymbol{r})$ is independent of R. We believe that this form of the free energy exactly represents the Ising model because a similar expression gives the exact free energy for fluid density derived by Grewe and Klein [33,34].

For dissipative Langevin dynamics the drift term $\Theta[\phi, \boldsymbol{r}]$ is proportional to $-\delta F/\delta\phi$ times a mobility M, which we are free to choose to correspond to the particular system of interest. We allow the mobility to be spatially varying. We take

$$\Theta[\phi, \boldsymbol{r}] = -M(\boldsymbol{r})\frac{\delta\widetilde{F}}{\delta\phi(\boldsymbol{r})}, \qquad (17)$$

where $\widetilde{F} \equiv F[\phi(\boldsymbol{r})]/R^d$ is the free energy per interaction volume for large R and is independent of R since $F[\phi(\boldsymbol{r})] \propto R^d$ [Eq. (14)]. The equation of motion, Eq. (5), becomes

$$\frac{\partial\phi(\boldsymbol{r},t)}{\partial t} = M(\boldsymbol{r})\{J(\Lambda * \phi)(\boldsymbol{r},t) - \beta^{-1}\,\text{arctanh}[\phi(\boldsymbol{r},t)] + h\}$$
$$+ \sqrt{B(\boldsymbol{r})}R^{-d/2}\eta(\boldsymbol{r},t)$$

(dissipative Langevin dynamics), (18)

where $B(\boldsymbol{r}) = 2M(\boldsymbol{r})\beta^{-1}$, as determined by a fluctuation-dissipation theorem. We numerically solve Eq. (18) with simulated noise in order to compare the relaxational Langevin dynamics with our predictions for stage two kinetics.

The dynamics in Eq. (18) evolves the system toward a local free-energy minimum which is a solution to the Euler-Lagrange equation $\delta F / \delta \phi = 0$,

$$\phi_0(\mathbf{r}) = \tanh[\beta J(\Lambda * \phi_0)(\mathbf{r}) + \beta h]. \quad (19)$$

To compare to the Glauber dynamics in Sec. IV C, we now expand about the background configuration to find equations for the evolution of the background configuration and the noise-driven fluctuations. Using the form of $\Theta[\phi, \mathbf{r}]$ given in Eq. (17), the nonlinear background dynamics in Eq. (10) becomes

$$\frac{\partial \phi_b(\mathbf{r},t)}{\partial t} = M(\mathbf{r})\{J(\Lambda * \phi_b)(\mathbf{r},t) - \beta_f^{-1} \operatorname{arctanh}[\phi_b(\mathbf{r},t)] + h\}, \quad (20)$$

and the linear theory for the fluctuations represented by Eq. (11) becomes

$$\frac{\partial \psi(\mathbf{r},t)}{\partial t} = M(\mathbf{r})\left[J(\Lambda * \psi)(\mathbf{r},t) - \beta_f^{-1} \frac{\psi(\mathbf{r},t)}{1 - \phi_b^2(\mathbf{r},t)} \right] + \sqrt{B(\mathbf{r})}\, \eta(\mathbf{r},t). \quad (21)$$

C. Glauber Langevin dynamics

There is a Langevin equation corresponding to the long-range Glauber Monte Carlo dynamics which is not equivalent to the dissipative Langevin dynamics of Eq. (18). This Glauber Langevin equation, derived in Ref. [35], is

$$\frac{\partial \phi(\mathbf{r},t)}{\partial t} = \tanh[\beta J(\Lambda * \phi)(\mathbf{r},t) + \beta h] - \phi(\mathbf{r},t) - \sqrt{B[\phi]} R^{-d/2} \eta(\mathbf{r},t), \quad (22)$$

where $B[\phi] = 2 - \tanh^2[\beta J(\Lambda * \phi)(\mathbf{r},t) + \beta h] - \phi^2(\mathbf{r},t)$ depends explicitly on $\phi(\mathbf{r},t)$ and the noise obeys the conditions in Eqs. (6) and (7). See also Ref. [36].

Glauber dynamics obeys detailed balance and therefore should take the system to equilibrium. We see that if we set the noise part of the dynamics equal to zero the system converges to a solution of the Euler-Lagrange equation,

$$\frac{\partial \phi_0(\mathbf{r})}{\partial t} = 0 = \tanh[\beta J(\Lambda * \phi_0)(\mathbf{r}) + \beta h] - \phi_0(\mathbf{r}), \quad (23)$$

in agreement with Eq. (19).

Following a quench to β_f and h_f the linearized equation for Glauber dynamics [Eq. (22)] from Eq. (11) is

$$\frac{\partial \psi(\mathbf{r},t)}{\partial t} = \{1 - \tanh^2[\beta_f J(\Lambda * \phi_b)(\mathbf{r}) + \beta_f h]\} J \beta_f(\Lambda * \psi)(\mathbf{r},t) - \psi(\mathbf{r},t) - \sqrt{B|_{\phi = \phi_b}}\, \eta(\mathbf{r},t). \quad (24)$$

When $\phi_b(\mathbf{r},t) \simeq \phi_0(\mathbf{r})$ we can apply Eq. (23) to Eq. (24) and obtain an expression for stage two kinetics,

$$\frac{\partial \psi(\mathbf{r},t)}{\partial t} = [1 - \phi_0^2(\mathbf{r})]\beta_f J(\Lambda * \psi)(\mathbf{r},t) - \psi(\mathbf{r},t) - \sqrt{2[1 - \phi_0^2(\mathbf{r})]}\, \eta(\mathbf{r},t). \quad (25)$$

Equation (25) for Glauber Langevin stage two dynamics is identical to Eq. (21) for the dissipative Langevin dynamics of stage two if the mobility is chosen to be

$$M(\mathbf{r}) = \beta_f[1 - \phi_0^2(\mathbf{r})]. \quad (26)$$

V. DISORDER-TO-ORDER TRANSITIONS

A. Theory

We first treat the transition from the disordered phase to either stripes or clumps in the antiferromagnetic Ising model. We consider dissipative dynamics [Eq. (22)] where we choose the mobility to obey Eq. (26), where $\phi_0(\mathbf{r}) = \phi_0$ so that $M(\mathbf{r}) = M$. For this choice, the dissipative dynamics and the Glauber dynamics should be equivalent for stage two.

For comparison we will also discuss the contrasting behavior of the ferromagnetic Ising model. In this case the initial background configuration is uniform and $\phi_b(t=0)$ may or may not be a solution to the Euler-Lagrange equation. Consider the uniform solutions to the Euler-Lagrange equation [Eq. (19)] given by

$$\phi_0 = \tanh[\beta(J\phi_0 + h)], \quad (27)$$

where we have used $\int d\mathbf{r} \Lambda(\mathbf{r}) = 1$. For $h = 0$, $\phi_0 = 0$ is a stable minimum for the antiferromagnet and the ferromagnet at high temperatures. For the ferromagnet at low temperatures and relatively small $|h|$, there is one solution unstable to $q = 0$ fluctuations and two solutions, either both stable or one stable and one metastable.

For the antiferromagnet at low temperatures and relatively small $|h|$ we know that the stable solution is not spatially uniform. The uniform unstable solution given by Eq. (27) is stable for the $q = 0$ mode and unstable for certain $q > 0$ modes. The details of the instability are discussed in the following.

The linearized equation for stage one kinetics is of the form of Eq. (21) with $\phi_b(\mathbf{r},t) = \phi_b(t)$. Equation (21) can be written in Fourier space as

$$\frac{\partial \psi(\mathbf{q},t)}{\partial t} = D(\mathbf{q},t)\psi(\mathbf{q},t) + \sqrt{B}\, \eta(\mathbf{q},t), \quad (28)$$

where

$$D(\mathbf{q},t) = M\left(J\Lambda(\mathbf{q}) - \frac{1}{\beta_f[1 - \phi_b^2(t)]} \right). \quad (29)$$

The solution to Eq. (28) is not an exponential in general but can be solved numerically by simultaneously solving Eq. (20) for $\phi_b(t)$.

Eventually, we expect that $\phi_b(t) \simeq \phi_0$ and that stage two kinetics takes over. The dynamics of the fluctuations is then given by Eq. (28) with $\phi_b(\mathbf{r},t) = \phi_0$, so that $D(\mathbf{q},t)$ for stage two kinetics becomes

$$D(\boldsymbol{q}) = \beta_f(1 - \phi_0^2)J\Lambda(\boldsymbol{q}) - 1. \tag{30}$$

With these simplifications, we solve Eq. (28) to obtain a generalization of Eq. (3) for disorder-to-order transitions,

$$S(\boldsymbol{q},t) = \frac{\delta(\boldsymbol{q})^2 \phi_0^2}{V} + \left[e^{2D(\boldsymbol{q})t}\left(S_0(\boldsymbol{q}) + \frac{1-\phi_0^2}{D(\boldsymbol{q})} \right) - \frac{1-\phi_0^2}{D(\boldsymbol{q})} \right], \tag{31}$$

where $S_0(\boldsymbol{q}) = \langle|\psi(t=t_0)|^2\rangle/V$ is determined by the initial conditions for the differential Eq. (28) and can be treated as a fitting parameter unless stage two kinetics begins immediately after the quench where $S_0(\boldsymbol{q}) = S(\boldsymbol{q},t=0)$. Equation (31) is only valid for stage two kinetics, that is, for $t > t_0$.

The sign of $D(\boldsymbol{q})$ in Eq. (30) determines whether the structure function grows or decays exponentially. To see for which $\boldsymbol{q}$ the value $D(\boldsymbol{q})$ first changes from negative to positive as the temperature is lowered to less than T_c, we look at the potential Λ in Fourier space. For the square-shaped interaction we have

$$\Lambda(q_x, q_y) = \frac{\sin(q_x)}{q_x}\frac{\sin(q_y)}{q_y}. \tag{32}$$

For the ferromagnet ($J = +1$), $D(\boldsymbol{q})$ for $\boldsymbol{q} = 0$ first crosses from negative to positive as the temperature is lowered. As the temperature is lowered for the antiferromagnetic case ($J = -1$), $D(q)$ first crosses from negative to positive at the global minimum of $\Lambda(\boldsymbol{q})$ which occurs at $\boldsymbol{q} = (\pm q^*, 0)$ or $\boldsymbol{q} = (0, \pm q^*)$ where $q^* \simeq 4.4934$. The temperature at which this crossover occurs is the critical temperature T_c for a given ϕ_0. The critical temperature for the antiferromagnetic system is

$$T_c = -\frac{\sin(q^*)}{q^*}(1 - \phi_0^2). \tag{33}$$

B. Simulation results

1. Critical quench

We first consider the critical quench for the antiferromagnet for which we expect stage two kinetics immediately following the quench (refer to Table I). For this case $M = \beta_f$ from Eq. (26). Figure 4 shows the correspondence among the linear theory prediction Eq. (31), the numerical solutions to the dissipative Langevin equation, Eq. (18), averaged over the noise, and the Monte Carlo simulations averaged over the noise. In Fig. 4 the structure factor is plotted versus q at an early time $t = 0.125$ MCS (Langevin time is measured in units of MCS). Because we use a square interaction, we plot

$$\bar{S}(q,t) \equiv [S(\pm q, 0; t) + S(0, \pm q; t)]/4 \tag{34}$$

instead of taking a circular average. For all simulations presented, we hold the ratio of the system size to the interaction range constant at $L/R \simeq 2.78$ so that the stripe state of the final phase is approximately commensurate with the system size [37].

The coarse graining employed in the Langevin equation allows us to consider system sizes and interaction ranges which are much larger than those of the Monte Carlo simu-
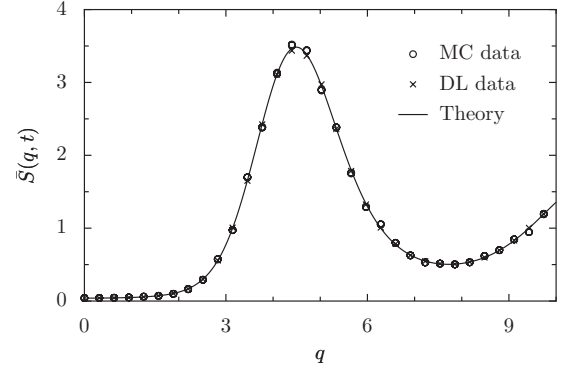

FIG. 4. Structure factor $\bar{S}(q,t) \equiv [S(\pm q, 0; t) + S(0, \pm q; t)]/4$ versus q for the antiferromagnetic Ising model for early time $t = 0.125$ MCS after a critical quench from $T_i = \infty$ to $T_f = 4T_c/9$. The Monte Carlo data (MC data) have an interaction range of $R = 128$, while the numerical solutions to the dissipative Langevin Eq. (18) (DL data) have a range of 10^6. The theory line is a plot of Eq. (31).

lations. In Fig. 4 the Monte Carlo simulations have $R = 128$ and the Langevin solutions have $R = 10^6$. The theory curve corresponds to an infinite interaction range (so that the linear theory lasts forever). Figure 4 shows that the linear theory is still a good approximation at time $t = 0.125$ for the Langevin and the Monte Carlo dynamics.

Next we compare the time dependence of $S(\boldsymbol{q},t)$ given by Eq. (31) following a critical quench to our Monte Carlo simulations. Figure 5 shows $\bar{S}(q,t)$ for $q \simeq q^*$ plotted against time for several values of R along with the theoretical prediction of Eq. (31). As predicted by Binder [20], we find that stage two kinetics holds for longer times as we increase the interaction range for this value of q.

2. Off-critical quenches

For external field quenches or off-critical temperature quenches we find that the short time behavior is independent of R and corresponds to our prediction of stage one kinetics. In Fig. 6 we present the results of off-critical quenches
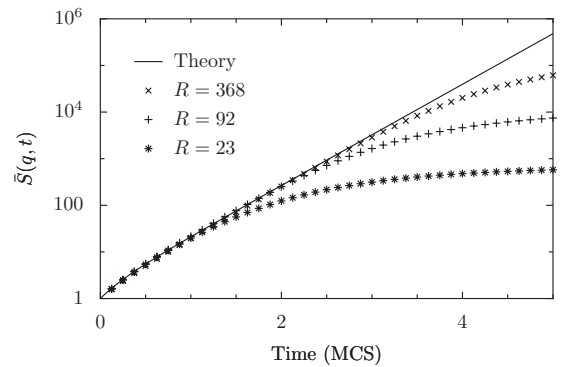

FIG. 5. Semilogarithmic plot of the structure factor $\bar{S}(q,t)$ for $q = 4.516 \simeq q^*$ versus time for our Monte Carlo simulations of a critical quench in the antiferromagnetic Ising model. The temperature is quenched from $T_i = \infty$ to $T_f = 4T_c/9$. The theory line is a plot of Eq. (31). The duration of the exponential growth increases as the interaction range increases.
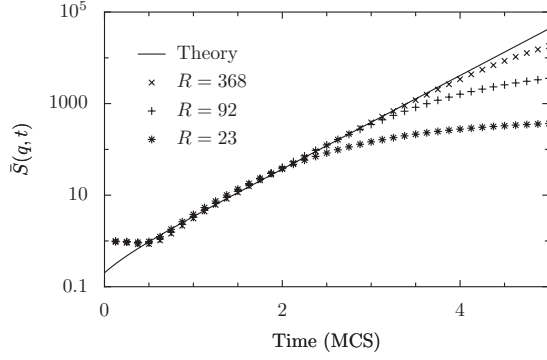
FIG. 6. Semilogarithmic plot of the structure factor $\bar{S}(q,t)$ for $q=4.516 \simeq q^*$ versus time for Monte Carlo simulations of an off-critical quench in the antiferromagnetic Ising model. The simulation parameters are $T_i=\infty$, $T_f=\frac{4}{9}T_c$, $h_i=0$, and $h_f=0.5$. The first Monte Carlo step is stage one kinetics, whose time scale is independent of interaction range. The duration of stage two kinetics, marked by exponential evolution, increases as the interaction range increases. The theory line is a plot of Eq. (31) [with $S_0(q)$ fit to the data] and is only expected to be applicable for stage two.

($T_i=\infty$, $h_i=0$, $T_f=4T_c/9$, and $h_f=0.5$) for $R=23$, 92, and 368 for Monte Carlo simulations averaged over at least 700 independent initial configurations for each value of R. We plot $\bar{S}(q,t)$ versus time for $q=4.516 \simeq q^*$. We interpret the first Monte Carlo step to be stage one kinetics, which, as we see from Fig. 6 has a time scale that is independent of the interaction range. At about 1 Monte Carlo step, stage two kinetics takes over and the structure factor at $q \simeq q^*$ grows exponentially until stage two kinetics breaks down. The break down occurs later for longer interaction ranges. These observations are consistent with the prediction that the time scale of stage one kinetics is determined by the noiseless dynamics of Eq. (10) which is independent of R. Note that stage one kinetics was not predicted by the CHC theory.

To show that our generalized theory predicts the same behavior for both the disorder-to-stripes and the disorder-to-clumps transitions, we compare $S_\perp(q,t)$ ($\boldsymbol{q}$ in the direction

perpendicular to the final stripe phase) and $S_\parallel(q,t)$ ($\boldsymbol{q}$ in the direction parallel to the final stripe phase) where $S_\perp(q,t)=S(q^*,0;t)$ and $S_\parallel(q,t)=S(0,q^*;t)$ for vertical stripes and $S_\perp(q,t)=S(0,q^*;t)$ and $S_\parallel=S(q^*,0;t)$ for horizontal stripes. We find that $S_\perp(q,t)$ and $S_\parallel(q,t)$ both grow exponentially with the same rate during stage two [see Fig. 7(a)]. It is not until after stage two that $S_\parallel(q,t)$ begins to decrease toward its final value. For comparison, $\bar{S}(q,t)$ is plotted in Fig. 7(b) for the disorder-to-clumps case. Note that the qualitative behavior for the disorder-to-stripes and the disorder-to-clumps transitions are the same.

VI. STRIPES-TO-CLUMPS TRANSITION

We now consider the unstable kinetics for spatial symmetry-breaking order-to-order transitions. In this section we develop a theory that describes the early time kinetics from an initial stripe state to the stable clump phase following an instantaneous quench of the external field. The development of the theory is analogous to that of the disorder-to-order case, but the periodic structure of the initial configuration of the system introduces some interesting deviations from the CHC theory.

A. Theory

After an external field quench with the temperature held constant, the stable solution to the Euler-Lagrange equation is a clump configuration corresponding to T_f and h_f (see Fig. 3). We find from numerical solutions to Eq. (18) that there is a second unstable stripe solution as well, $\phi_s(\boldsymbol{r})=\phi_s(r_x)$ where r_x and r_y represent scaled spatial coordinates (we assume here that the stripes are in the vertical direction).

As in Sec. V, we proceed by considering dissipative dynamics [Eq. (22)] where we choose the mobility to obey Eq. (26), where we now choose $\phi_0(\boldsymbol{r})=\phi_s(r_x)$ so that $M(\boldsymbol{r})=M(r_x)$. Again, the dissipative dynamics and the Glauber dynamics should be equivalent for stage two.

The nonlinear dynamics of Eq. (10) evolves the initial stripe configuration $[\phi_b(r_x,r_y;t=0)=\phi_b(r_x;t=0)]$ toward
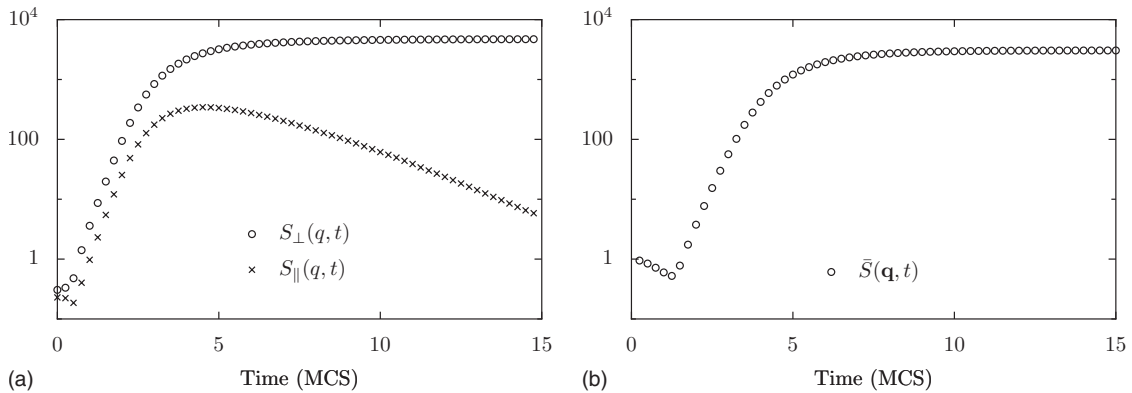

FIG. 7. (a) A semilogarithmic plot of $S_\perp(q,t)$ (where $\boldsymbol{q}$ is in the direction perpendicular to the final stripe phase) and $S_\parallel(q,t)$ (where $\boldsymbol{q}$ is in the direction parallel to the final stripe phase) versus time for an off-critical quench from disorder to stripes with $T_f=0.07$, $h_f=0.4$, and $R=92$. Stage two lasts until about 1.5 MCS, after which $S_\perp(q,t)$ and $S_\parallel(q,t)$ begin to separate and eventually $S_\parallel(q,t)$ decreases toward its stable value. (b) A semilogarithmic plot of $\bar{S}(q,t)$ for an off-critical quench from disorder to clumps with $T_f=0.02$, $h_f=0.8$, and $R=92$ is plotted for comparison.

$\phi_s(r_x)$. When $\phi_b(r_x,t) \simeq \phi_s(r_x)$, stage two kinetics begins. In this case stage two kinetics is given by Eq. (21) where the mobility $M(r_x)$ is given by Eq. (26) with $\phi_0(\boldsymbol{r}) = \phi_s(r_x)$ and $J = -1$. We find that in order to determine the time dependence of the structure factor for stage two, it is sufficient to consider the dynamical Eq. (21) without the noise term,

$$\frac{\partial \psi(\boldsymbol{r},t)}{\partial t} = -M(r_x)(\Lambda * \psi)(\boldsymbol{r},t) - \psi(\boldsymbol{r},t). \qquad (35)$$

To understand the behavior of the Fourier modes we Fourier transform Eq. (35),

$$\frac{\partial \psi(q_x,q_y;t)}{\partial t} = -\int dq_x' M(q_x' - q_x)\Lambda(q_x',q_y)\psi(q_x',q_y;t) \\ - \psi(q_x,q_y;t). \qquad (36)$$

Note that in Eq. (36) the q_y modes (along the direction of the stripes) are decoupled but the q_x modes (perpendicular to the direction of the stripes) are not. Hence the Fourier modes do not have purely exponential growth as in the disorder-to-order case.

To solve Eq. (36) numerically, we discretize space. For a lattice with $L \times L$ coarse-grained bins, and therefore $L \times L$ Fourier modes, we write $\psi(q_x,q_y)$ as ψ_{ij}, where q_x and q_y are $q_x = 2\pi i/L$ and $q_y = 2\pi j/L$ for $0 \le i,j < L$. Because the q_y variables are decoupled, we choose a particular value $j = j_0$ for the remainder of the calculation. The discretized Eq. (36) can be written in matrix form

$$\frac{\partial \psi_i(t)}{\partial t} = A_{ik}\psi_k(t), \qquad (37)$$

where we have left off the $j = j_0$ index. The matrix A is real and has elements

$$A_{ik} = -M_{ik}\Lambda_k - \delta_{ik}. \qquad (38)$$

To solve the homogeneous set of equations, $\partial \psi_i(t)/\partial t = A_{ik}\psi_k(t)$, we diagonalize A to find eigenvectors v^α which satisfy

$$A_{ik}v_k^\alpha = \lambda^\alpha v_i^\alpha, \qquad (39)$$

where the index $\alpha = 1, 2, \ldots, L$. If the eigenvalues λ^α are real and distinct (which we have found to be true for the matrices we have numerically diagonalized) then v^α form a new basis. We expand ψ in this basis,

$$\psi_i(t) = \sum_\alpha a^\alpha(t)v_i^\alpha. \qquad (40)$$

Equation (37) becomes

$$\frac{\partial}{\partial t}\sum_\alpha a^\alpha(t)v_i^\alpha = \sum_\alpha a^\alpha(t)\lambda^\alpha v_i^\alpha. \qquad (41)$$

Because v^α are linearly independent, Eq. (41) can be written as a set of equations,

$$\frac{\partial}{\partial t}a^\alpha(t) = a^\alpha(t)\lambda^\alpha, \qquad (42)$$

with solutions

$$a^\alpha(t) = a^\alpha(0)e^{\lambda^\alpha t}. \qquad (43)$$

The structure factor $S(q_x = 2\pi i/L, q_y = 2\pi j_0/L; t) = S_{ij_0}(t) = \langle |\phi_{ij_0}(t)|^2 \rangle / V$ due to the noiseless dynamics is

$$S_{ij_0}(t) = \frac{\phi_{s,i}^2(\delta_{0,i})^2}{V} + \sum_{\alpha,\alpha'} \frac{\langle a^\alpha(0)a^{\alpha'}(0)\rangle}{V}e^{(\lambda^\alpha + \lambda^{\alpha'})t}v_{ij_0}^\alpha v_{ij_0}^{\alpha'}, \qquad (44)$$

where $\phi_{s,i} = \phi_s(q_x = 2\pi i/L)$ and we expect that $\langle a^\alpha(0)a^{\alpha'}(0)\rangle \sim V$. In the unstable regime, there is at least one positive λ^α indicating exponential growth. From Eq. (44) we see the exponential growth lasts throughout stage two but it is the growth of eigenvectors that will, in general, mix Fourier modes. We expect, however, that after some time the term in the sum in Eq. (44) which corresponds to the largest positive eigenvalue will dominate, and the growth of Fourier modes will be well approximated by pure exponential growth. Note that we only expect to see exponential growth for near-mean-field systems whose long interaction ranges extend the lifetime of the stage two kinetics to $\tau \sim \ln R$ at the fastest growing eigenvector.

B. Simulation results

1. External field quench

We present the results of Monte Carlo simulations for a quench from a stable stripe configuration with $h_i = 0$ to $h_f = 0.8$ at $T_i = T_f = 0.04$. Snapshots following this quench are shown in Fig. 8 for a system with $L = 1024$ and interaction range $R = 368$. We find that the stripes quickly become less dense and then narrower. Finally, around 10 MCS, the stripes begin to form clumps, and the modulation along the length of the clumps becomes visually perceptible.

In Fig. 9 we show $S(\boldsymbol{q},t)$ at various values of $\boldsymbol{q}$. We find that the growth is most rapid along the line of modes for which $q_y = 0$ and the line of modes which is closest to $q_y \simeq q^*$ (the peak of the Fourier transform of the interaction potential). In Fig. 9 the Monte Carlo data are averaged over at least 700 initial stripe configurations for the same parameters as the system shown in Fig. 8. We look at several q_x modes with $q_y \simeq q^*$. There is a steep initial increase in $S(q_x,q_y)$ and then a gradual decrease during the first Monte Carlo step, which we interpret as stage one kinetics toward the unstable state stripe solution. Stage one corresponds to the initial behavior of the stripes seen in Fig. 8 followed by narrowing of the stripes. Eventually the structure factor modes grow exponentially before stage two kinetics breaks down at around 10 MCS. Two distinct exponential rates are evident.

In Fig. 10 we compare the evolution of the structure factor for systems with different interaction ranges. We see that the time scale of stage one kinetics is independent of the interaction range, and the exponential behavior lasts longer for larger R, as in the CHC theory.

2. Understanding stage two kinetics

To better understand the behavior of the system during stage two, we seek an analogy to the critical quench where

(a) t=0.125   (b) t=5.00
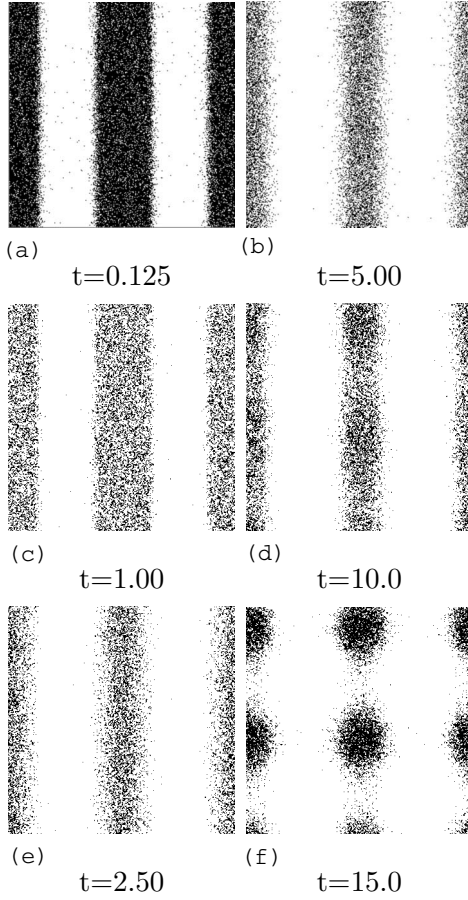
(c) t=1.00   (d) t=10.0

(e) t=2.50   (f) t=15.0

FIG. 8. Several snapshots showing the initial evolution from an unstable stripe configuration to a clump configuration in the antiferromagnetic Ising model. The lattice size is 1024, the interaction range is 368, and $T_i=T_f=0.04$. Time is measured in Monte Carlo steps beginning after the external field quench from $h_i=0$ to $h_f=0.8$. The corresponding structure factor is shown in Fig. 9.

stage one is entirely absent from the early unstable evolution. Thus, instead of quenching the field, we will initially prepare our system in the state corresponding to the unstable Euler-Lagrange solution.

We verify numerically that the unstable stripe solution $\phi_s(r_x, r_y)$ to the Euler-Lagrange equation at a particular T and h corresponds to the *one-dimensional* stable clump solution $\phi_{1D}(r_x)$ with the same temperature and external field: $\phi_s(r_x, r_y) = \phi_s(r_x) = \phi_{1D}(r_x)$.

For the stripes-to-clumps transition we used the $h_f=0.8$ and $T_f=0.04$. We find the stable one-dimensional solution by numerically solving Eq. (18) in one dimension at this field and temperature. We use the corresponding unstable stripe solution $\phi_s(r_x)$ to find the matrix A in Eq. (38) which depends on $\phi_s(r_x)$ through the mobility $M(r_x) = \beta_f[1 - \phi_s(r_x)^2]$.

For the parameters considered ($h_f=0.8$, $T_f=0.04$, $L=1024$, and $L/R \simeq 2.78$), we diagonalize A and find two positive eigenvalues of Eq. (39). (Larger lattice sizes give a larger number of positive eigenvalues. The depth of the quench also affects the number of positive eigenvalues.) We also find by examining the eigenvectors corresponding to these two positive eigenvalues that each Fourier mode has a nonzero contribution from only one of the two positive ei-
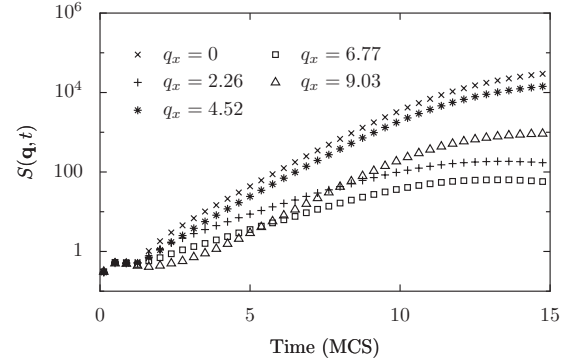

FIG. 9. Semilogarithmic plot of the structure factor $S(\mathbf{q}, t)$ versus time in the antiferromagnetic Ising model with $R=368$ for various values of q_x for $q_y \simeq q^*$ following a quench from $h_i=0$ to $h_f=0.8$ at $T_i=T_f=0.04$. The Monte Carlo data are averaged over about 700 independent stripe configurations. We interpret the first Monte Carlo step to be stage one kinetics. After this time stage two takes over. At the beginning of stage two, the Fourier modes do not grow exponentially. Eventually they grow exponentially at two different rates (starting from about 4 Monte Carlo steps). This exponential growth lasts until about 10 Monte Carlo steps for $R=368$.

genvalues. Thus we expect each Fourier mode to be dominated by one of the two exponential terms with a positive argument, and two distinct exponential growth rates should eventually be apparent. This is consistent with the data shown in Figs. 11 and 12.

The one-dimensional solution is used to construct initial two-dimensional configurations for the Monte Carlo simulations. The length of the one-dimensional coarse-grained lattice is chosen to be the same as the length of the two-dimensional Monte Carlo lattice. We use the value of $\phi_s(r_x)$ to determine the probability that the corresponding Ising spin is initially up: $p = [\phi_s(r_x) + 1]/2$. We repeat this process over all horizontal strips of the Ising lattice. We then run the Monte Carlo simulation and monitor $S(\mathbf{q}, t)$ for various values of $\mathbf{q}$, averaging over independent runs. As expected, the evolution looks similar to the evolution of the corresponding $S(\mathbf{q}, t)$ in Fig. 9 with about the first Monte Carlo step re-
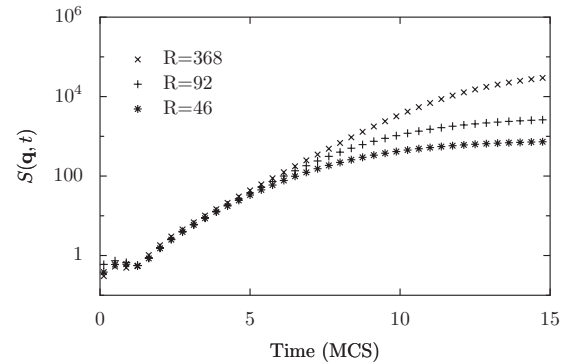

FIG. 10. Semilogarithmic plot of the structure factor $S(\mathbf{q}, t)$ at $q_x=0$ and $q_y \simeq q^*$ versus time in the antiferromagnetic Ising model for interaction ranges $R=46$, 92, and 368. The quench parameters are the same as those in Fig. 9. We find that the time scale of stage one kinetics (about the first MCS) is independent of R, and the exponential evolution of stage two lasts longer for longer R.
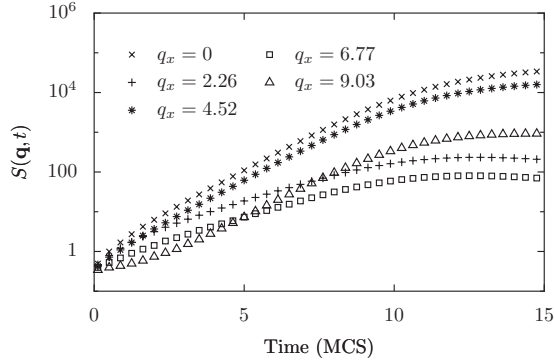
FIG. 11. Semilogarithmic plot of the structure factor versus time in the antiferromagnetic Ising model for various q_x values with q_y =4.518. The initial configuration is constructed from the one-dimensional solution ϕ_{1D} to the Euler-Lagrange equation at temperature $T=0.04$ and field $h=0.8$. Data are averaged over about 700 independent stripe configurations. Two distinct exponential growth rates are apparent from about 3 to 8 Monte Carlo steps.

moved. In Fig. 12 we have plotted two Fourier modes from Fig. 11 along with the exponential curves from Eq. (44) to indicate the growth rates predicted from our matrix calculation.

After some initial evolution the Fourier modes eventually grow exponentially at one of the two rates, reflecting the coupling of the modes due to the spatial variation in the initial state. The fact that our theory predicts exponential growth rates even though we did not consider the effect of the noise on the structure factor indicates that, as in the disorder-to-order case, the contribution from the noise term has the same time dependence as the noiseless part, at least at later times during stage two [38].

VII. SUMMARY AND DISCUSSION

We have presented a generalization of the linear theory of Cahn and Hilliard [16–18] and Cook [19] for the early stage unstable evolution. In particular, we have given a description of the initial unstable evolution for transitions with spatial symmetry breaking and no order-parameter conservation. One of our predictions is that there are two stages of early time kinetics in general for systems with long interaction ranges. Stage one is dominated by a symmetry-preserving nonlinear dynamics and takes the system to a symmetry-constrained local minimum of the free energy on a time scale that is independent of the interaction range. Although noise-driven fluctuations may also be growing during stage one, they do not evolve significantly in this relatively short-lived regime. In stage two these noise-driven fluctuations break the spatial symmetry of the initial configuration and grow for an extended period of time.

This picture is consistent with the observed behavior of the long-range antiferromagnetic Ising model, a system that exhibits several symmetry-breaking transitions. We find the stage two kinetics of the long-range antiferromagnetic Ising model is characterized by long-lived exponential growth of symmetry-breaking fluctuations. For the disorder-to-order
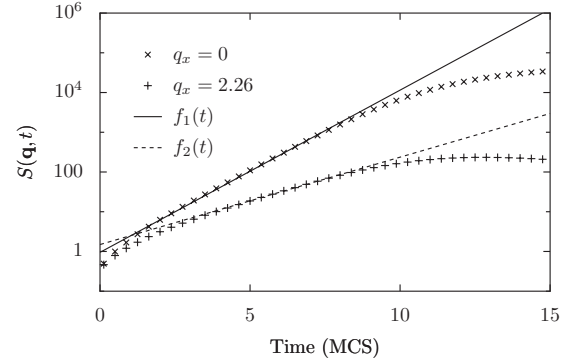

FIG. 12. A semilogarithmic plot of structure factor for two Fourier modes from Fig. 11 along with predictions for linear theory exponential growth, $f_1(t) \sim \exp(2\lambda_1 t)$ and $f_2(t) \sim \exp(2\lambda_2 t)$, where the S intercept has been fitted to the data. Here λ_1 and λ_2 are the two positive eigenvalues from our matrix calculation.

case the symmetry-breaking fluctuations are individual Fourier modes. In contrast, the order-to-order case is complicated by the spatial symmetry of the initial configuration, which couples the growth of the Fourier modes. For this reason the symmetry-breaking fluctuations in the order-to-order case are not individual Fourier modes but eigenvectors in Fourier space. The evolution of the Fourier modes is described by linear combinations of exponential growth and/or decay, which after some time resembles pure exponential growth due to the largest positive eigenvalue.

We have focused on systems without order-parameter conservation. A future publication will apply our generalized theory for order-to-order transitions with order-parameter conserving dynamics.

Our results have several consequences for experimentalists and simulators looking to fit their data to a linear theory after an unstable quench. For disorder-to-order transitions stage two kinetics, which is analogous to the CHC theory, is expected immediately after the quench only for systems with conserved order parameters or only in special circumstances for systems with no conserved order parameters (as in a critical quench). For order-to-order transitions, exponential growth of Fourier modes is delayed for two reasons. In stage one exponential growth is not expected. In stage two the evolution of Fourier modes is represented by a linear combination of exponential terms, and therefore only approximate exponential evolution is expected after some time. Because the lifetime of stage two kinetics is limited by the finite interaction range, exponential Fourier mode growth may be absent even if the linear evolution of stage two is present.

[1] J. W. Christian, *The Theory of Transformations in Metals and Alloys* (Pergamon, Oxford, 2002), Vols. 1 and 2.

[2] F. S. Bates and G. H. Fredrickson, Annu. Rev. Phys. Chem. **41**, 525 (1990).

[3] M. Seul and D. Andelman, Science **267**, 476 (1995).

[4] T. Garel and S. Doniach, Phys. Rev. B **26**, 325 (1982).

[5] D. Lacoste and T. C. Lubensky, Phys. Rev. E **64**, 041506 (2001).

[6] C. Harrison, D. H. Adamson, Z. Cheng, J. M. Sebastian, S. Sethuraman, D. A. Huse, R. A. Register, and P. M. Chaikin, Science **290**, 1558 (2000).

[7] C. Roland and R. C. Desai, Phys. Rev. B **42**, 6658 (1990).

[8] R. A. Wickham, A.-C. Shi, and Z.-G. Wang, J. Chem. Phys. **118**, 10293 (2003).

[9] G. H. Fredrickson and K. Binder, J. Chem. Phys. **91**, 7265 (1989).

[10] M. Li, Y. Liu, H. Nie, R. Bansil, and M. Steinhart, Macromolecules **40**, 9491 (2007).

[11] B. Yu, B. Li, P. Sun, T. Chen, Q. Jin, D. Ding, and A.-C. Shi, J. Chem. Phys. **123**, 234902 (2005).

[12] M. Nonomura and T. Ohta, J. Phys.: Condens. Matter **13**, 9089 (2001).

[13] J. D. Gunton, M. San Miguel, and P. S. Sahni, *Phase Transitions and Critical Phenomena* (Academic, New York, 1983), Vol. 8.

[14] P. C. Hohenberg and B. I. Halperin, Rev. Mod. Phys. **49**, 435 (1977).

[15] The ferromagnetic Ising model with no external field has an up or down spin symmetry which is broken in the final low-temperature state. This symmetry breaking should not be confused with *spatial* symmetry breaking, which is not present in the ferromagnetic Ising model.

[16] J. W. Cahn and J. E. Hilliard, J. Chem. Phys. **28**, 258 (1958).

[17] J. W. Cahn and J. E. Hilliard, J. Chem. Phys. **31**, 688 (1959).

[18] J. W. Cahn, Trans. Metall. Soc. AIME **242**, 166 (1967).

[19] H. E. Cook, Acta Metall. **18**, 297 (1970).

[20] K. Binder, Phys. Rev. A **29**, 341 (1984).

[21] In analogy to the ferromagnetic case we refer to dynamics as conserving or not conserving the "order parameter" even though $\hat{\phi}$ is not a well-defined order parameter for the antiferromagnetic Ising model which we will consider.

[22] W. Klein, H. Gould, N. Gulbahce, J. B. Rundle, and K. Tiampo, Phys. Rev. E **75**, 031114 (2007).

[23] D. W. Heermann, Phys. Rev. Lett. **52**, 1126 (1984).

[24] D. W. Heermann, Z. Phys. B: Condens. Matter **61**, 311 (1985).

[25] T. Izumitani and T. Hashimoto, J. Chem. Phys. **83**, 3694 (1985).

[26] M. Okada and C. C. Han, J. Chem. Phys. **85**, 5317 (1986).

[27] B. Morin, K. R. Elder, and Martin Grant, Phys. Rev. B **47**, 2487 (1993).

[28] We note that Corberi *et al.* found evidence of two early growth stages in ϕ^4 models as well [F. Corberi, A. Coniglio, and M. Zannetti, Phys. Rev. E **51**, 5469 (1995)]. In these cases, stage one kinetics acts to smooth the fluctuations of the initial conditions.

[29] K. Barros, R. Dominguez, and W. Klein, e-print arXiv:0810.3949, Phys. Rev. E (to be published).

[30] M. E. J. Newman and G. T. Barkema, *Monte Carlo Methods in Statistical Physics* (Oxford University Press, Oxford, 1999).

[31] W. Klein, H. Gould, R. A. Ramos, I. Clejan, and A. I. Mel'Cuk, Physica A **205**, 738 (1994).

[32] M. Kac, G. E. Uhlenbeck, and P. C. Hemmer, J. Math. Phys. **4**, 216 (1963).

[33] N. Grewe and W. Klein, J. Math. Phys. **18**, 1729 (1977).

[34] N. Grewe and W. Klein, J. Math. Phys. **18**, 1735 (1977).

[35] K. Barros and W. Klein (private communication).

[36] A. D. Masi, E. Orlandi, E. Presutti, and L. Triolo, Nonlinearity **9**, 53 (1996).

[37] The ratio L/R gives the approximate number of stripes (or clumps along one dimension) in the system. We have tested many values of L/R and found that the early stage two kinetics is unaffected by this value. We did find that stage two lasts longer for larger values of L/R. At any value of L/R larger interaction ranges extend the lifetime of stage two. We do not deal with the creation of defects in systems with large L/R because the defects do not form until after stage two breaks down.

[38] That the contribution from the noise term has the same time dependence as the noiseless term can be shown to be true in the case where $B = $const [from Eq. (2)] but is complicated by further couplings for a spatially dependent B.